How membrane lipids influence plasma delivery of reactive oxygen species into cells and subsequent DNA damage: An experimental and computational study

Jonas Van der Paal[1], Sung-Ha Hong[2,3], Maksudbek Yusupov[1], Nishtha Gaur[2], Jun-Seok Oh[4,5], Robert D. Short[6], Endre J. Szili[2] and Annemie Bogaerts[1]

[1] Research Group PLASMANT, Department of Chemistry, University of Antwerp, Belgium
[2] Future Industries Institute, University of South Australia, Adelaide, SA 5095, Australia
[3] Centre for Plasmas and Fluids, Department of Physics and Engineering, The Australian National University, Canberra, Australia
[4] Department of Physical Electronics and Informatics, Osaka City University, Osaka, 558-8585 Japan
[5] BioMedical Engineering Center (BMEC), Graduate School of Engineering, Osaka City University, Osaka, 558-8585 Japan
[6] Material Science Institute, Lancaster University, Lancaster LA1 4YW, United Kingdom

Abstract

The mechanisms of plasma in medicine are broadly attributed to plasma-derived reactive oxygen and nitrogen species (RONS). In order to exert any intracellular effects, these plasma-derived RONS must first traverse a major barrier in the cell membrane. The cell membrane lipid composition, and thereby the magnitude of this barrier, is highly variable between cells depending on type and state (e.g. it is widely accepted that healthy and cancer cells have different membrane lipid compositions). In this study, we investigate how plasma-derived RONS interactions with lipid membrane components can potentially be exploited in the future for treatment of diseases. We couple phospholipid vesicle experiments, used as simple cell models, with molecular dynamics (MD) simulations of the lipid membrane to provide new insights into how the interplay between phospholipids and cholesterol may influence the response of healthy and diseased cell membranes to plasma-derived RONS. We focus on the (i) lipid tail saturation degree, (ii) lipid head group type, and (iii) membrane cholesterol fraction. Using encapsulated molecular probes, we study the influence of the above membrane components on the ingress of RONS into the vesicles, and subsequent DNA damage. Our results indicate that all of the above membrane components can enhance or suppress RONS uptake, depending on their relative concentration within the membrane. Further, we show that higher RONS uptake into the vesicles does not always correlate with increased DNA damage, which is attributed to ROS reactivity and lifetime. The MD simulations indicate the multifactorial chemical and physical processes at play, including (i) lipid oxidation, (ii) lipid packing, and (iii) lipid rafts formation. The methods and findings presented here provide a platform of knowledge that could be leveraged in the development of therapies relying on the action of plasma, in which the cell membrane and oxidative stress response in cells is targeted.

1. Introduction

Targeted cell membrane therapy has the potential to shape the future of how we treat and manage chronic diseases such as cancers. In order to continue improving cell membrane therapies, it is necessary to improve our fundamental understanding of how the unique features of diseased *versus*

healthy cell membranes can be exploited for treatment of the disease with minimal damage to healthy cells and tissue. Indeed, in a wide range of diseases, the cell membrane composition is altered and membrane function is perturbed.[1,2] New approaches for the treatment of chronic diseases, including cancers, target these perturbations in membrane composition and function.[2] For example, cancer cells display a higher phosphatidylethanolamine (PE) content in the outer leaflet of the bilayer membrane, as they lose their ability to maintain PE asymmetry in both leaflets of the plasma membrane.[3] Raised PE content enhances the susceptibility of the cell membrane to perforation in response to peptide-based anticancer therapy and has been shown to lead to eventual cell death.[4] Another relatively new strategy is the use of molecular drugs, such as Minerval® (2-hydroxyoleic acid), which interfere with lipid structures within the cell membrane to kill cancer cells.[5]

When focussing on targeted membrane therapy, a major issue still to be addressed is to increase our understanding of how the complex interplay between the array of membrane lipids and other membrane components influences the cell response to the treatment. This problem is exacerbated by the fact that there are more than 1000 different lipids in any eukaryotic cell.[6,7] On one hand, the overall structure of the membrane is determined by the chemical structure of each of these individual lipids. The fluidity of the membrane, for example, increases when introducing lipids which contain shorter lipid tails, unsaturated cis-double bonds, and decreases when cholesterol is added to the system.[8] On the other hand, the overall composition of a membrane is only one part of the picture. As the lipids are free to move throughout the plane of the membrane, lipids with long saturated carbon tails and cholesterol molecules tend to cluster together due to strong van der Waals interactions, leading to the formation of transient microdomains or rafts.[8]

In the development of therapeutics that leverage on differences in cell membranes, the starting point has been to focus on the (currently known) few global differences in the membrane lipid composition between a diseased (e.g. cancerous) cell and its healthy equivalent cell.[1] Indeed, it is widely known that the development of cancerous cells is accompanied with alterations in the lipid composition of the plasma membranes of these cells. Multiple studies already revealed a significant overlap between the fluidity of plasma membranes and the malignancy of cells.[9–11] More specifically, cancerous cell membranes, in comparison to their healthy counterpart are typically characterised by (i) a higher number of aquaporin channels [12,13], (ii) altered levels of cholesterol [9,11,14], (iii) increased levels of unsaturated lipids [9,14], and (iv) increased expression of certain lipid types in the outer membrane (e.g. PE as mentioned above).[3,11] These unique features of cancer cells are currently being investigated as potential targets for anticancer therapies. This is particularly applicable for therapies that induce oxidative stress in cancer cells (e.g. chemotherapy, radiation therapy and in the context of this study, plasma therapy) through the production of reactive oxygen species (ROS), which (once inside the cell) can lead to biochemical changes in the cell such as irreversible DNA damage, resulting in eventual cell death.[15]

An exciting feature of plasma as a cancer treatment therapy, versus radiation therapy, is that plasma is non-ionising and is therefore more likely to be “gentler” on bystander (non-cancerous) cells.[16,17] Furthermore, it is possible to scale down the plasma beam to the single-cell-level, enabling highly-targeted treatment.[18,19] Plasma devices are also much more affordable: for instance, current

commercial medical plasma devices retail as low as few tens of thousands of USD, which is significantly less than the costs of new linear accelerators of around 1M USD.

Identifying the exact mode of action of cold atmospheric pressure plasmas (CAPs) on tumours or individual cells (healthy and cancer cells) remains, however, one of the largest challenges in the field of plasma medicine.[20] On the biological side, a large number of parameters must be taken into account, including e.g., intracellular processes and the extracellular matrix. On the physical side, CAPs can be seen as a very reactive cocktail of many different ingredients, including highly reactive species, electric fields, neutral atoms or molecules, ions, photons and electrons. The main mode-of-action of plasma jets (a class of CAPs) in treating cancers is thought to arise from the rich mixture of ROS and reactive nitrogen species (RNS) delivered by plasma jets into cells and tissue, targeting the destruction of cancer cells and tumours through oxidative stress.[20–22] These include, e.g., the hydroxyl radical ($^{\bullet}OH$), oxygen atoms (O), hydrogen peroxide (H_2O_2), peroxynitrite ($ONOO^-$) and the superoxide anion (O_2^-). In order to induce a certain cellular response, these molecules need to either (i) modify the extracellular matrix, which subsequently interacts with cells, (ii) modify the cell membrane itself, or (iii) enter the cell directly to induce intracellular modifications. Whichever mode-of-action, it is clear that the outer cell membrane is involved in the transmission of the signal into cells.

Owing to the complexity of cell membranes, simple models usually comprising one or two phospholipid types have been developed to gain new insights into the role of specific cell membrane components in regulating cellular processes, both experimentally, e.g. with phospholipid vesicle cell models, and by computational simulations of lipid bilayers.[23] These model systems have also been utilised to study the response of specific components of the cell membrane to oxidative stress. For example, it was observed that the membrane of phospholipid vesicles is more prone to destabilisation through oxidation processes when the membrane cholesterol content is below 50 mol% [24], and molecular dynamic (MD) simulations of lipid peroxidation products have revealed that at reduced levels of cholesterol, membranes are less capable of self-repair from physical damage induced by oxidation of the membrane lipids.[25]

This present study aims to provide new insight into how plasma-derived RONS interact with vesicles comprising different lipid components of relevance for treating diseases such as cancers. By experiment and computational modelling, we investigate how ROS interact and penetrate vesicles comprising different proportions of saturated and unsaturated lipids, and how the addition of cholesterol and changes in phospholipid (PL) head group influence these interactions and the transport of ROS to the vesicle interior. The subsequent ability of ROS to induce DNA damage within the vesicles is measured using a molecular beacon (MB). Vesicles were subjected to a mixture of ROS, generated using a CAP jet. These jets are being intensively investigated for cancer therapies with promising patient outcomes already seen in initial clinical case studies.[26] Vesicle experiments are supported by umbrella sampling (US) MD simulations, investigating the effect of the membrane composition on the permeation of H_2O_2, which is known to be one of the major longer-lived ROS generated by CAP jets in aqueous liquids [27], and is itself an important cellular signalling molecule.[28]

2. Experimental

2.1 General set-up

Figure 1 illustrates the CAP jet treating vesicles in solution with the location of the voltage probe, current monitor and the spectrometer for optical emission spectroscopy (OES).

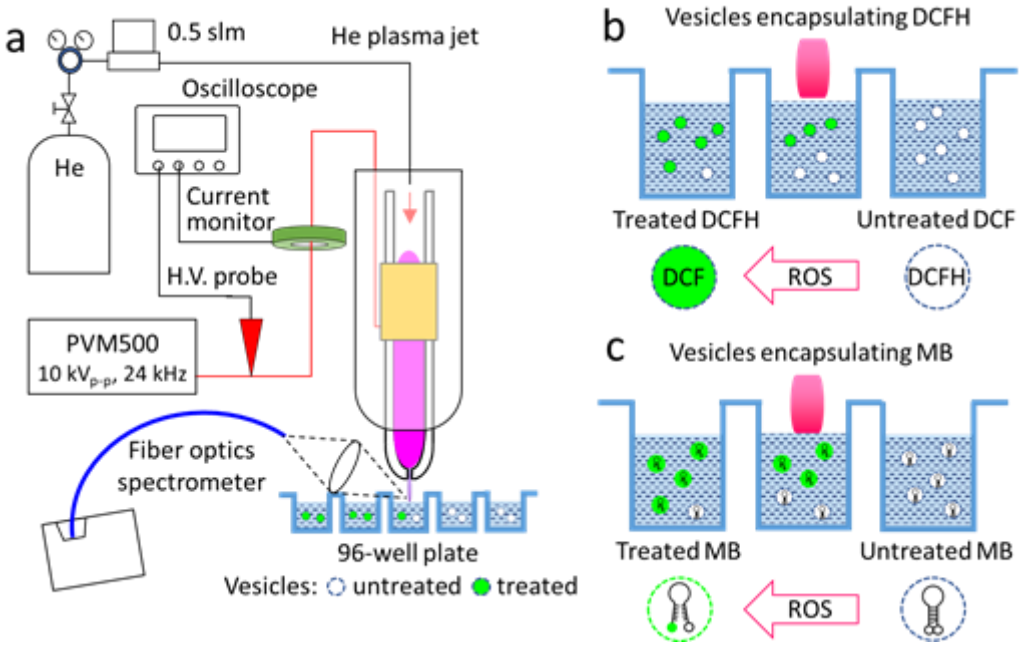

Figure 1: (a) Illustration of the CAP jet configuration used for the treatment of the vesicles, and the location of the voltage and current probes and OES for the plasma diagnostics. Illustration of the induction of fluorescence in vesicles containing (b) encapsulated 2,7-dichlorodihydrofluorescein (DCFH) or (c) MB.

The CAP jet was described in detail elsewhere.[29] A grounded plate was placed below the 96-well plate, which served as a counter electrode for the powered ring electrode. Helium (He) gas (BOC, high purity grade) flow was fixed at 0.5 standard litres per minute (slpm) throughout all experiments using a digital mass flow controller (Apex, 0–2 slpm flow range). A sinusoidal voltage of 10 kVp–p (peak-to-peak) at 24 kHz was applied to the external electrode with a PVM500 power supply (Information Unlimited). The treatment distance, measured between the nozzle of the CAP jet and the top of the 96-well plate, was fixed at 3 mm.

The applied voltage and current were measured using a ground-referenced high voltage probe (Pintek Electronics, HVP-18HF) directly connected to the HV cable and a current monitor (Pearson 2877) placed around the insulated part of the high voltage cable. The discharge current was determined by subtracting the current measured during operation of the CAP jet from the baseline current measured with applied voltage but without helium flow (i.e. without CAP discharge).

A fibre optic spectrometer (OceanOptics, Model – Flame-TX-R1-ES, Grating – #31-500/250) was used for measuring the optical emission between 200-1000 nm. All the measurements were taken in a custom-built “dark box” to prevent interference from ambient light.[29] The optical emission from the

plume of the CAP jet was recorded during treatment of the vesicle solutions. The integration time of the spectrometer (T) was set to 100 ms.

2.2 Phospholipid vesicle synthesis

Ten different vesicle compositions were synthesized, which all contained different concentrations of 1,2-dioleoyl-*sn*-glycero-3-phosphocholine (DOPC), 1,2-dipalmitoyl-*sn*-glycero-3-phosphocholine (DPPC), 1,2-dipalmitoyl-*sn*-glycero-3-ethanolamine (DPPE), and cholesterol. All compositions are shown in Table 1.

Table 1: Composition of the synthesised phospholipid vesicles

Mixture	Cholesterol (mol%)	DOPC (mol%)	DPPC (mol%)	DPPE (mol%)
1	10	0	85	5
2	15	0	80	5
3	25	0	70	5
4	10	85	0	5
5	15	80	0	5
6	25	70	0	5
7	25	0	75	0
8	25	0	50	25
9	25	75	0	0
10	25	50	0	25

These specific lipids were chosen, as lipids containing a phosphatidylcholine (PC) head group are the most common lipids in all cellular membranes (up to almost 60 mol% in specific membranes).[14,30,31] Moreover, C18 lipids are also one of the most abundant fraction of lipids found in cellular membranes, both in healthy cells, as well as in cancerous cells.[14,31] Furthermore, lipids containing a phosphatidylethanolamine (PE) head group were added to this study as certain diseased cells, such as cancer cells, display a higher phosphatidylethanolamine (PE) content in the outer leaflet of the bilayer membrane.[3,11] Lastly, by investigating DOPC, DPPC and DPPE, we were able to systematically alter one lipid parameter (head group or saturation degree), while keeping all others fixed.

The concentrations of DPPE were chosen because the PE concentration in the cell membrane is approximately 25%. [30] In healthy cells, all PE lipids are in the inner leaflet, but cancer cells lose the ability to maintain this asymmetry, with PE being expressed also in the outer leaflet. [4] In this study, we assume that the RONS will affect the outer leaflet first. Therefore, we chose to mimic the increasing concentration of PE in the outer leaflet of cancer cells up to 25 mol%. The concentration of cholesterol investigated in this study is also based on concentrations observed in human cells. [32]

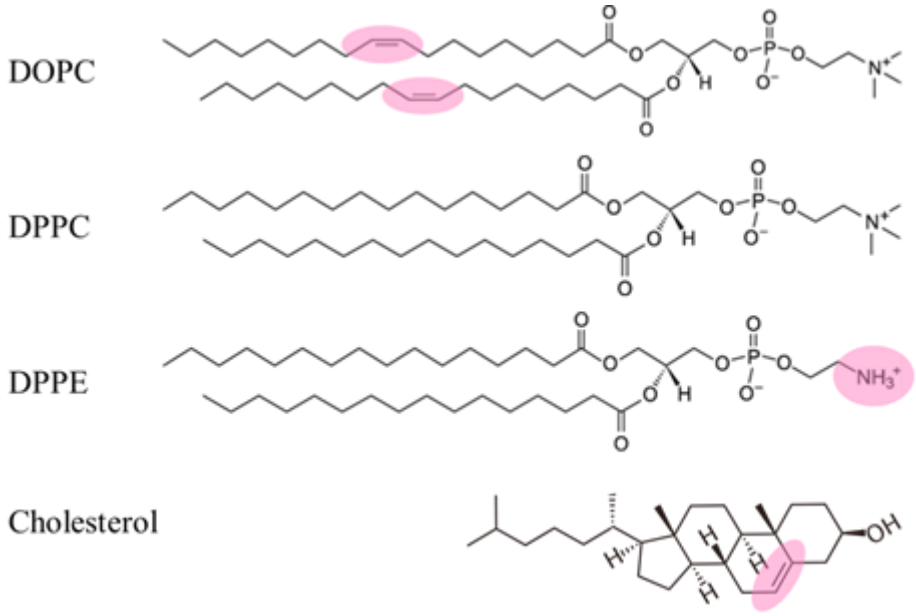

Figure 2: Schematic representation of the structures of DOPC, DPPC and DPPE lipids, and cholesterol. The parts highlighted in pink indicate key differences in the structure of each molecule that was tested in this study.

The different lipid compositions used in the ten vesicle types synthesized allowed us to tailor (i) the saturation degree of the phospholipid membranes with DOPC and DPPC, (ii) the cholesterol fraction within the membranes, and (iii) the size of the lipid head group with DPPE (which has a relatively small lipid head group compared to DOPC and DPPC). The key features of DOPC, DPPC, DPPE and cholesterol that were tested in this study are shown in Figure 2.

The vesicles were synthesized by mixing 100 µL of a 0.1 mM stock solution of each vesicle mixture with 200 µL of chloroform, after which the solutions were dried with nitrogen gas until only a thin film of the lipids on the bottom of the vial was left. Afterwards, 2.5 mL of the pre-prepared MB or DCFH solution was added, and the mixture was heated to 70 °C for 10 min for DCFH or 50 °C for the MB (lower temperature to prevent unwanted conformational changes to the MB). Subsequently, the mixture was extruded 15 times through two 100 nm polycarbonate membranes in a hand-held syringe extruder (Avanti Polar Lipids, model # 610000). This extruded solution was then transferred to a Sephadex G25 column, to purify the mixture and remove non-encapsulated dye. Finally, the eluate was stored overnight at 4°C. Before CAP jet treatment, the vesicles were diluted by adding 4 mL of 4-(2-hydroxyethyl)piperazine-1-ethanesulfonic acid (HEPES) to the solution. The details of the buffers used in this synthesis can be found in Appendix A1.

2.3 2,7-dichlorodihydrofluorescein (DCFH): assessment of ROS ingress into vesicles

A 1 mg/mL DCFH solution was prepared by dissolving 5 mg of DCFH-diacetate (Sigma-Aldrich, catalogue number D6883) in 5 mL of neat ethanol. This solution was stored at -18 °C until use. Ester hydrolysis was induced by adding 500 µL of the DCFH solution to 2 mL of a 10 mM sodium hydroxide solution and incubating at 25 °C for 30 min at ambient temperature, before adding 10 mL of HEPES buffer to neutralise the solution.

2.4 Molecular beacon (MB): assessment of DNA strand breaks

The MB consisted of a single-stranded loop and double-stranded stem structure with a fluorophore and quencher moiety at the end of each DNA strand. With the MB intact, the quencher inhibits fluorescence of the fluorophore. If the DNA strand of the MB breaks, the quencher is separated from the fluorophore, resulting in a switch-on of fluorescence (as a positive indication of DNA strand breaks).[33] A 37 nM of MB (Sigma Aldrich, 3017672631, FAM-5-GCACTGAAGCGCCGCACGCCATGTCGACGCG-CTTCAGTGC–3′-BHQ-1), as supplied in each bottle, was dissolved in 372 μL of 10 mM Tris-base buffer (pH 7.6), giving a final concentration of 0.1 mM. To ensure the correct configuration of the MB, the solution was first heated to 95 °C to (reversibly) denature the DNA, after which the MB was incubated overnight in the dark at ambient temperature, allowing the MB structure to slowly reform to its correct configuration. The MB solution was further diluted (1:5) in HEPES leading to a final working concentration of 16.7 μM for encapsulation within the vesicles.

2.5 Microplate reader measurements

After CAP jet treatment of the 200 μL test solutions, 100 μL of the solution was transferred to a fresh 96-well plate for absorbance or fluorescence measurements on a BMG Labtech Fluostar Omega microplate reader. Fluorescence of the MB or DCFH was recorded at an excitation wavelength of 485 nm and emission wavelength of 520 nm. Absorbance of ortho-phenylenediamine (OPD) was measured at a wavelength of 450 nm for determination of H_2O_2 concentrations (Appendix A2). Unless otherwise stated, all samples were measured directly after treatment. Where applicable, the normalised intensities were calculated by dividing the measured intensity of the test (CAP jet treated) solution by the non-treated solution.

2.6 Simulation: H_2O_2 delivery across different membrane compositions

We performed MD simulations to study the permeation of H_2O_2 across lipid bilayers with various compositions. Although CAPs generate many different RONS, we choose to focus on H_2O_2 as (i) we demonstrated in our previous work [34,35] that all polar RONS behave in the same way as H_2O_2, and (ii) as the vesicles are treated in a liquid solution, so a large fraction of the short-lived RONS generated by the plasma jet (e.g., $^{\bullet}$OH) will recombine before reaching the vesicles, making H_2O_2 the most abundant reactive species present in the solution. As in the experiments, ten different bilayers were constructed, of which the composition was chosen to mimic the composition of the vesicles studied experimentally, i.e., the bilayers contained different concentrations of DPPE and cholesterol in DPPC or DOPC systems. All these bilayers contained a total of 128 lipids, hydrated by 6000 water molecules surrounding the bilayer structure on both sides. The MD simulations thus only included a small patch of a membrane, which then served as a model system for the entire vesicle. The construction of the systems, as well as the equilibration procedure and the details of the US simulations, are provided in Appendix B1 and B2, respectively.

2.7 Simulation: Area per lipid calculation

The surface area per lipid was determined by dividing the total surface area of the membrane (averaged over the 200 ns, by sampling the data after every 200 ps) by the number of lipids of one leaflet of the phospholipid bilayer (PLB) (i.e., Lx × Ly/64, where Lx and Ly are the x and y dimensions of the PLB, respectively, and 64 is the number of lipids present in one layer).

2.8 Simulation: Radial distribution function calculation

The radial distribution function (RDF) determines the probability of finding a particle at a certain distance from a fixed reference particle. We calculated the RDF between phosphorus atoms of neighbouring DOPC molecules in membranes containing either 0 or 25% DPPE, using the last 200 ns of the equilibration run (by sampling the data after every 200 ps) and applying the *gmx rdf* tool of GROMACS.

2.9 Statistical analysis

Statistical analysis was performed on the data presented in figures 4, 6 and 7, using an unpaired Student t-test assuming unequal variances. A *p* value of less than 0.05 or 0.001 was considered to be significantly different (95% and 99.9% confidence, respectively).

3. Results and discussion

3.1 CAP jet as a source of oxidative molecules

The basic electrical and optical properties of the CAP jet were characterised in order to determine how the physicochemical properties of the CAP jet relate to the delivery of ROS into the vesicle solution. Figure 3a shows the voltage and current waveforms during CAP jet treatment of a vesicle solution. The same voltage waveform with amplitude of 10 kV_{p-p} at 24 kHz was maintained for all of the experiments (Figure 3a). Figure 3a also shows the typical positive and negative discharge current peaks expected for a dielectric barrier discharge CAP jet.[36] The average discharge power was calculated to be 0.79 W.

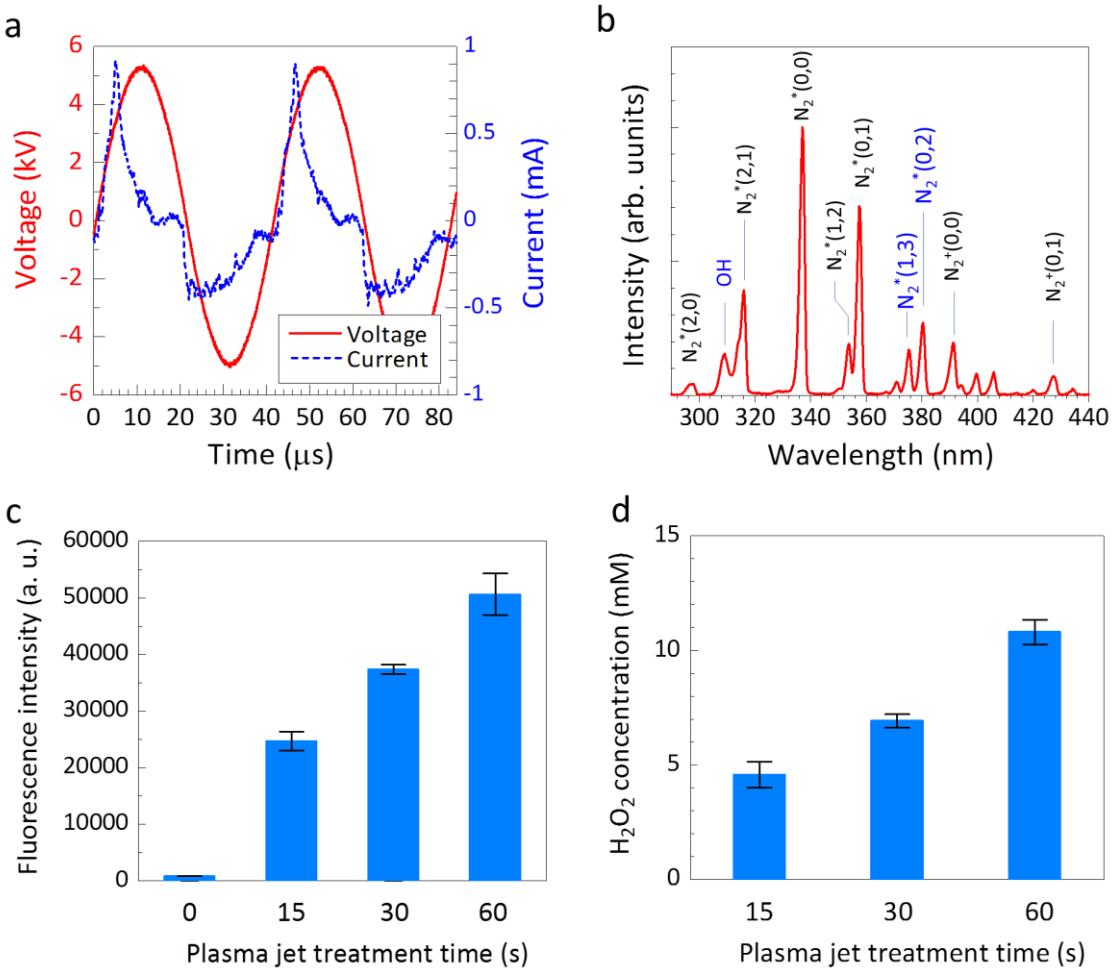

Figure 3: Electrical and optical characteristics of the CAP jet and its generation of oxidative molecules in HEPES buffer. (a) Applied voltage and current waveforms at 10 kV_{p-p} and 24 kHz; (b) optical emission spectrum profile between 280–440 nm; (c) ROS and RNS generated in HEPES with the CAP jet, as measured by fluorescence of the DCFH molecular probe after oxidation by ROS and RNS; (d) H_2O_2 concentrations generated in HEPES with the plasma jet as measured by the OPD/HRP molecular probe system.

Optical emission spectroscopy (OES) was used to determine the high-energy components of the CAP jet that facilitate ROS (and RNS) chemistry. Figure 3b shows a typical optical emission spectrum profile of the CAP jet during treatment of the vesicle solution including the N_2 2nd positive system ($C^3\Pi_u$–$B^3\Pi_g$) and the N_2^+ 1st negative system ($B^2\Sigma_u^+$–$X^3\Sigma_g^+$) between 300-400 nm, and the $^{\bullet}$OH at 308 nm.[37] Using the theoretical calculation of the N_2 2nd positive system [N_2^*(1,3) and N_2^*(0,2)] with the spectrum simulator of the N_2^* 2nd positive system kindly provided by Professor Hiroshi Akatsuka at Tokyo Institute of Technology [38], we obtained the best fitted spectra with the rotational temperature (T_r) of 0.028 eV. T_r is considered the gas temperature because of the rapid rotational relaxation through inelastic collisions between molecules and atoms[39], and was calculated to be 290 K. Here, the T_r of N_2 molecules is in very good agreement with our previous calculations.[40–42] The vibrational temperature (T_v) of 0.28 eV was higher than our previous studies. This is probably due to the higher frequency of 24 kHz used to operate the CAP jet in this study compared to our previous studies (below 10 kHz), which probably resulted in increased inelastic collisions between electron and

N_2 molecules in the ambient air. In Figure 3b, a prominent peak is seen at 308 nm representative of the $^{\bullet}OH$, which is a key species that can produce longer-term ROS chemistry in solution, particularly through recombination of neighbouring $^{\bullet}OH$ molecules producing H_2O_2 [43,44]. H_2O_2 can persist in solution on the timescale of days or longer.[45,46]

We used DCFH as a broad range molecular probe for ROS (and RNS) molecules to qualitatively determine the CAP jet production of these molecules in the buffered solution. As shown in Figure 3c, the fluorescence of DCFH (after oxidation by ROS and RNS) increased as function of the CAP jet treatment time. As mentioned above, H_2O_2 is usually the most abundant longer-lived ROS generated by CAP jets in solution. Figure 3d shows that the concentration of H_2O_2 increased as function of CAP jet treatment time in the concentration range 4-12 mM. We anticipated that this H_2O_2 concentration range would be sufficient to observe changes in the vesicles.[47]

3.2 ROS delivery into vesicles with different membrane compositions

Having established that the vesicles remained intact after plasma jet treatment (Appendix A4), we next set out to study how different components of the vesicle membranes influence the ingress of ROS into the vesicle interior. Enhanced ingress of ROS into biological cells induces a higher level of oxidative stress on the cells, and excessive or sustained levels of ROS are toxic to all cells, which for some applications can be used for the targeted destruction of cells (e.g. in cancer therapy).[48] The specific membrane components studied were: (i) unsaturated and saturated phospholipids; (ii) cholesterol fraction; and (iii) DPPE. For these experiments, DCFH encapsulated within the vesicles was used as a fluorescence probe for detection of ROS (and RNS).

3.3 ROS delivery across cell membranes

Oxidation of non-fluorescent DCFH to fluorescent DCF was used to qualitatively measure the amount of ROS that had entered vesicles after CAP jet treatment. In the context of the CAP jet used herein, H_2O_2 is produced in abundance in the mM range; other molecules such as nitrate (NO_3^-) and nitrite (NO_2^-) are produced at much lower concentrations in the μM range. We looked at (i) the effect of the saturation degree of the phospholipids, (ii) the cholesterol fraction and (iii) the amount of DPPE included within the membrane. Below, the experimental results of synthetic vesicles are combined with MD simulations for all three elements separately.

- **Effect of lipid tail saturation degree**

To examine the effect of the saturation degree of the phospholipids on the ROS ingress in vesicles, vesicles were synthesised to incorporate equal amounts of cholesterol and DPPE, and contain either DOPC (C18:1) or DPPC (C16:0); i.e., we compare vesicle systems 1-3, 7 and 8 (containing DPPC) with systems 4-6, 9 and 10 (based on DOPC) (Table 1). The results are illustrated in Figure 4.

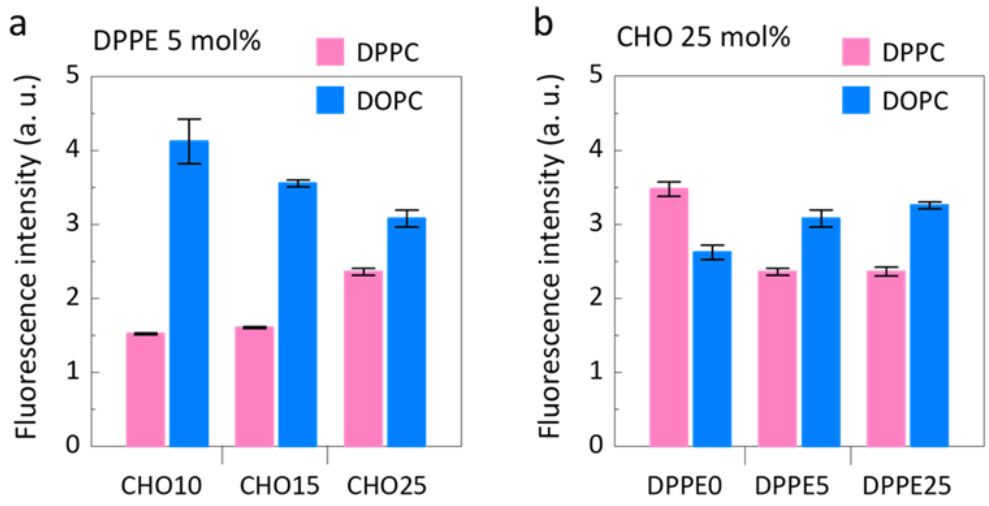

Figure 4: Effect of either DPPC or DOPC on the ingress of ROS into vesicles following 60 s of CAP jet treatment. The vesicles in the left graph contain different concentrations of cholesterol (10, 15 or 25 mol%) with fixed concentration of DPPE (5 mol%), whereas the vesicles in the right graph contain different concentrations of DPPE (0, 5 and 25 mol%) at fixed cholesterol concentration (25 mol%).

With a single exception in the case where vesicles contain no DPPE (discussed in following paragraph), Figure 4 shows that there is greater ingress of ROS in the vesicles containing DOPC (i.e., the unsaturated lipids) when compared to those containing DPPC ($p < 0.001$), for which two likely explanations can be found. First, DOPC has a lower phase transition temperature of 256 K compared to DPPC (314 K).[49] Therefore, at an average temperature of approximately 298 K, the membrane containing DOPC will be much more fluid compared to that containing DPPC, which could facilitate the passive diffusion of ROS into the vesicle interior. The second explanation is that the double bond within the lipid tails of DOPC presents a potential site for lipid oxidation, with highly-reactive ROS that reach the vesicle membrane (the oxidation rate of unsaturated hydrocarbons by $^{\bullet}OH$ is 10 to 20 times higher compared to that of saturated hydrocarbons).[50] Oxidation increases (i) the polarity of the membrane interior (in extreme cases even aqueous pores can be formed [34,51]) and (ii) the fluidity of the membrane; both are expected to facilitate passive diffusion of polar ROS and RNS, such as, H_2O_2, NO_2^- or NO_3^-, as previously demonstrated.[34] Figure 4 also indicates one exception, i.e., for membranes containing the highest amount of cholesterol (25 mol%) and the lowest amount of DPPE (0 mol%). In this case, the DPPC-containing membrane was more susceptible to ROS permeation than the DOPC membrane. This is attributed to the opposite effects that cholesterol and DPPE exert in either saturated (DPPC) or unsaturated (DOPC) membranes, and will be discussed in more detail in the later sections, in which we focus on the effect of both cholesterol and DPPE separately.

MD simulations of PLBs were performed to investigate the importance of DOPC and DPPC on ROS ingress. The obtained free energy profiles (FEPs) for H_2O_2 (major ROS produced by the CAP jet in this study) are shown in Figure 5, which are a measure for the barrier of passive diffusion of H_2O_2 across the membrane.

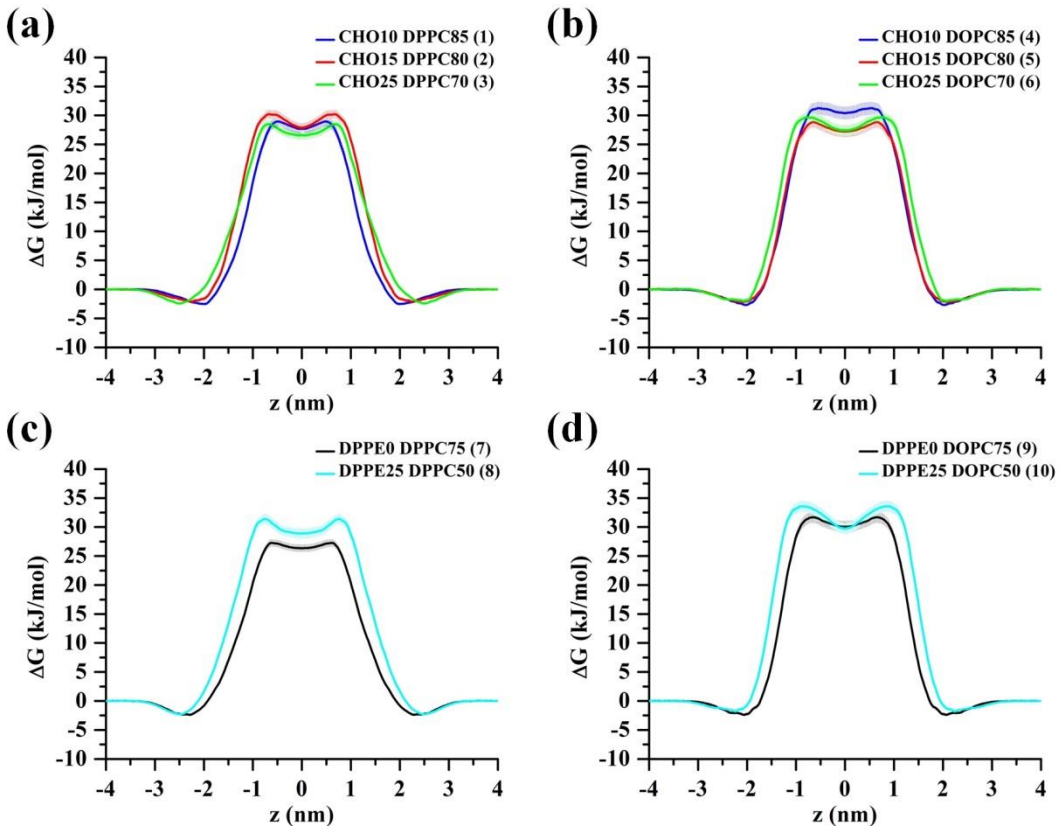

Figure 5: FEPs obtained from the US simulations for all different membrane compositions. The numbers mentioned in the legend indicate the molar fraction of each component in the lipid bilayer. (a) and (b) compare the effect of DPPC and DOPC, respectively, when varying the cholesterol content (keeping the DPPE content fixed at 5 mol%), whereas in the membranes investigated in (c) and (d) the DPPE content is varied, keeping the cholesterol content fixed at 25 mol%, for either (c) DPPC or (d) DOPC.

To understand what these Figures show, we take Figure 5a as an example. The y ordinate shows the increase in free energy (delta G) as a single molecule of H_2O_2 is introduced to the system. z = 0 nm is defined as the centre of the PLB, whereas the head groups of the lipids can be found at $z \approx \pm 2$ nm. At $z \approx \pm 4$ nm there is no change in free energy anymore, as the H_2O_2 molecule is located in the bulk of the liquid. As we move the H_2O_2 molecule from the bulk of the liquid towards the lipid membrane, the free energy of the system increases, which is due to the hydrophilic nature of H_2O_2, in comparison to the hydrophobic environment of the lipid membrane. A local minimum in free energy is observed in the centre of the membrane, which is due to a decreased lipid density in this region.[51]

Figure 5 shows almost no difference between the height of the FEPs of bilayers containing either DOPC or DPPC (comparing Figure 5a with 5b, or Figure 5c with 5d). This means that the passive diffusion rate across all these membranes would be almost identical. This indicates that the differences observed in the vesicle experiments are more likely to arise from lipid oxidation occurring at the unsaturated bonds in DOPC, and not due to differences in fluidity (arising from differences in phase transition temperature). An important note, however, is that these simulations only focus on the diffusion of H_2O_2, thereby ignoring other smaller species (e.g. the $^{\bullet}OH$), which will be discussed later in more detail.

- **Effect of cholesterol**

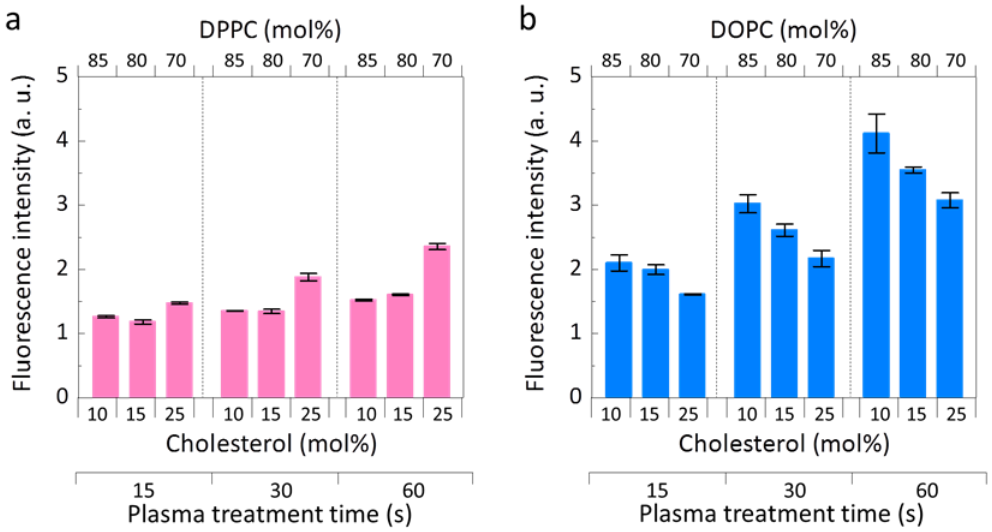

Figure 6: Effect of cholesterol membrane content on the ingress of ROS during CAP jet treatment of (a) DPPC or (b) DOPC vesicles. The DPPE content is fixed at 5 mol%.

To determine the effect of variations in the cholesterol content on ROS delivery, vesicle systems 1 to 6 (Table 1) were compared; these vesicles contained 10, 15 or 25 mol% cholesterol in combination with 5 mol% DPPE, and either DOPC or DPPC. The results of the DCFH measurements are shown in Figure 6.

First, these graphs illustrate opposite trends in vesicles containing mostly either (a) DPPC or (b) DOPC. In the DPPC-containing vesicles (pink bars), ROS ingress is increased with increasing cholesterol fraction, while in the DOPC membranes (blue bars), the opposite trend is seen. Specifically, at lower cholesterol fractions of 10 and 15 mol%, a significantly higher amount of ROS was detected in the DOPC vesicles ($p < 0.001$). On the other hand, the difference in the amount of ROS detected in both vesicles was insignificant ($p > 0.05$) at the highest cholesterol fraction of 25 mol% (due to ROS ingress increasing for DPPC vesicles and decreasing for DOPC vesicles at the highest cholesterol fraction). Moreover, Figure 6 shows that in the case of the DOPC vesicles, in comparison to the DPPC vesicles, (i) the overall ROS ingress is higher, as was also clear from Figure 4; but also that (ii) the increase in ROS ingress upon increasing treatment time is much more pronounced. Indeed, the fluorescence intensity in each of the DPPC vesicles is almost constant as a function of treatment time, while the DOPC vesicles show a clear increase with increasing treatment time from 15 s up to 60 s. This corresponds with our conclusion above; i.e., that the ingress in the DOPC vesicles is mostly governed by lipid oxidation, which facilitates permeation of the membrane, and the latter increases upon longer treatment time, while in the DPPC-containing vesicles, only a small accumulation of ROS due to passive diffusion is observed.

An explanation as to why opposing trends are observed upon altering the cholesterol fraction in either DPPC or DOPC vesicles can also be found in the ability of CAP jet species to oxidize these different lipids.[50] In DPPC vesicles lacking cholesterol, oxidation is not likely to occur.[52]

However, when cholesterol is added to the membrane, the unsaturated bonds present in these molecules can be oxidized by impinging ROS. Due to this oxidation, the polarity of the membrane core would increase slightly, which facilitates further permeation of CAP jet-derived ROS.[53] Therefore, if the concentration of cholesterol increases in the DPPC vesicles, the permeation of ROS increases as well, as is observed in Figure 6. In DOPC vesicles, on the other hand, even without the presence of cholesterol, lipid oxidation already occurs due to the double bond in the lipid tails. Replacing DOPC by cholesterol reduces the total number of reactive sites per vesicle present in the lipid core (each molecule of DOPC contains two double bonds, whereas cholesterol only contains one double bond), thereby lowering the overall reactivity of the membrane. This explains why a reduced amount of intracellular ROS is measured in the DOPC vesicles upon increasing cholesterol fraction (Figure 6). Furthermore, the rigid nature of cholesterol also strongly increases the lipid packing in unsaturated membranes, which would hamper passive ROS permeation further, as previously shown.[25]

- **Effect of DPPE content**

The effect of the concentration of DPPE on the ingress of plasma-derived ROS, was examined using vesicles containing 0, 5 or 25 mol% of DPPE. Throughout these experiments, the cholesterol content was fixed at 25 mol%. The results of the broad-range ROS measurements are shown in Figure 7.

Adding DPPE to the vesicles clearly exerts the opposite effect to that of adding cholesterol (cf. Figure 6 to 7); i.e., adding DPPE leads to a decreasing permeability in the DPPC vesicles, but an increase of ROS ingress in the DOPC vesicles. The effect of DPPE on ROS ingress is particularly noticeable when comparing vesicles with 5 mol% and 25 mol% DPPE. At 5 mol% DPPE, ROS ingress between DPPC and DOPC is not significant ($p > 0.05$), whereas a significantly ($p < 0.05$) higher amount of ROS ingress was observed for DOPC vesicles at 25 mol% DPPE (compared to DPPC vesicles). In the DPPC vesicles, lipid tail oxidation effects are not expected to play any role, as DPPC and DPPE contain identical lipid tails (Figure 2). Therefore, differences observed may be explained by structural changes between DPPC and DPPE, i.e., a different head group of the lipid. Indeed, DPPC contains a phosphatidylcholine (PC) group (PO_4^--$N(CH_3)_3^+$), whereas DPPE contains a phosphatidylethanolamine (PE) group (PO_4^--$N(H_3)_3^+$) (Figure 2).

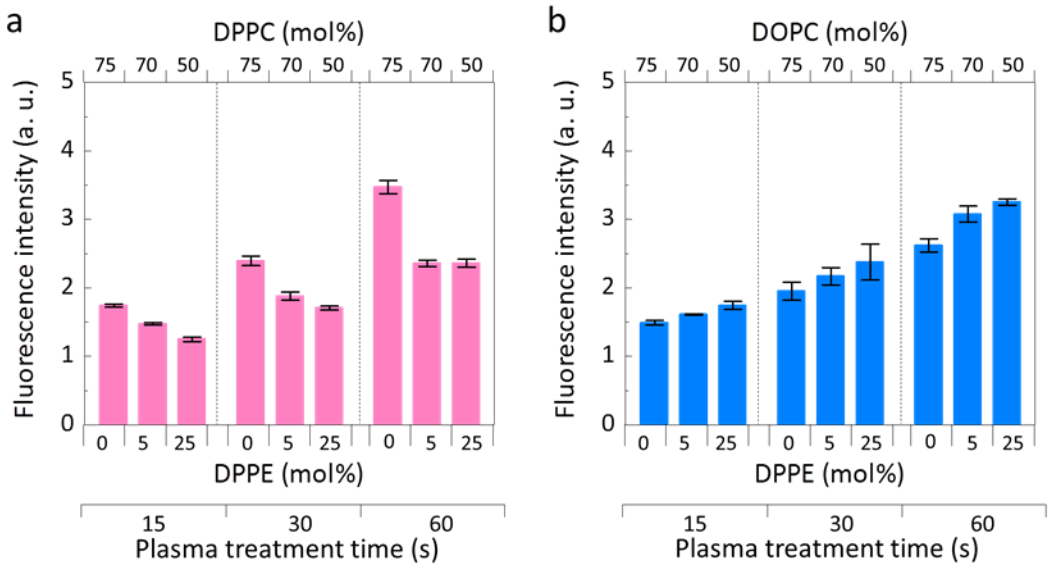

Figure 7: Effect of DPPE content on the ingress of CAP-jet derived ROS into (a) DPPC or (b) DOPC vesicles. The cholesterol content was fixed at 25 mol%.

The PE head group of DPPE is less bulky than the PC head group in DPPC. Thus, when replacing DPPC by DPPE, the lipids can be packed closer together, which makes passive permeation of ROS more difficult, as indeed observed in the DCFH measurements. This is also confirmed in the MD simulations, by comparing the average area per lipid in the different membrane structures, as shown in Table 2.

Table 2: Calculated values of the area per lipid for the different simulated membranes.

Vesicle type	**Area per lipid (nm^2)**	
	0 mol% DPPE	25 mol% DPPE
DPPC	0.451 ± 0.004	0.435 ± 0.001
DOPC	0.506 ± 0.002	0.449 ± 0.001

Increasing the DPPE content in either the DPPC or the DOPC vesicles increases the packing of the lipids, leading to a decreasing area per lipid (Table 2). Upon increasing the DPPE fraction, the passive diffusion of ROS should be hampered in both systems. For the DPPC vesicles, this is also observed in the US simulations, which show that upon increasing DPPE fraction, the free energy barrier of H_2O_2 permeation increases (see Figure 5c).

However, in the DOPC vesicles, the DCFH measurements indicate an increasing permeability upon increasing DPPE fraction, which does not correlate with the results in Table 2. The explanation for this is not straightforward, even more so when we consider that when DOPC is replaced by DPPE, the total number of reactive sites in the membrane decreases, which should result in a decrease in the likelihood of pore formation due to lipid oxidation, and thereby also the chances of ROS permeating the membrane. Therefore, we suspect that a different effect is taking place, which counteracts the effects of both an increase in lipid packing density and a decrease in lipid oxidation.

One possibility is that the presence of DPPE leads to the creation of lipid rafts in the membrane structures, i.e.; lipids of the same type pack together to form patches with an enhanced local concentration of this lipid inside the membrane. It is known that cholesterol tends to form such rafts together with sphingolipids and other saturated lipids.[8,54] These saturated lipids contain an aliphatic tail, which is also present in DPPE (see Figure 2), but not in DOPC (which contains a double bond in each lipid tail). Therefore, upon increasing the DPPE concentration, lipid rafts could be generated, containing elevated levels of DPPE and cholesterol. As the overall molar fraction of each lipid type is fixed in the vesicles, this would mean that other parts of the vesicle membrane are enriched in DOPC. Thus, due to the generation of lipid rafts, enriched in DPPE and cholesterol, other parts of the membrane might be enriched in DOPC, which serve as the 'weak spot' of these membranes, being extremely vulnerable to pore formation upon lipid oxidation. In previous research, we have shown that in order to create pores in lipid membranes, very high lipid (local) oxidation degrees are required[16], which can indeed only occur if these oxidised lipids are grouped together in membrane patches.

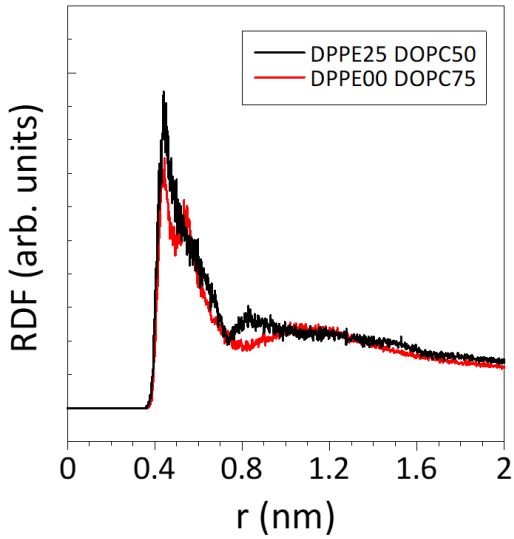

Figure 8: RDFs of the P-P distance of neighbouring DOPC lipids in systems containing 0 or 25 mol% DPPE. The numbers mentioned in the legend indicate the molar fraction of each component in the vesicles. The cholesterol content is fixed at 25 mol%.

To analyse possible lipid raft formations in these membrane structures, we compare the radial distribution functions (RDFs) of the P-P distance of neighbouring DOPC lipids, in systems containing 0 and 25 mol% DPPE in Figure 8. These RDFs are a measure for the probability of finding a particle (in this case, any P-atom) at a certain distance from a fixed reference particle (the reference P-atom).

In the system containing only DOPC and cholesterol (red curve), the first peak (at a distance of 0.45 nm) corresponds to two DOPC molecules placed next to each other. The second peak, at a distance of 0.55 nm, most likely occurs from DOPC molecules separated by a cholesterol molecule. Upon adding DPPE to the system, the black curve clearly shows that the peak of neighbouring DOPC molecules increases, which means that more DOPC molecules are grouped together. At first sight, this is counterintuitive, as there are more non-DOPC lipids in the system, so the chance of DOPC being

organised directly next to each other should decrease. Therefore, these results might indicate that lipid raft formation does occur in these systems, creating rafts that are either enriched in DOPC (explaining this higher peak) or in DPPE/cholesterol. As mentioned before, these DOPC rafts serve as the membrane's 'weak spot' for lipid oxidation and pore formation, which explains the increased ROS ingress in Figure 7 upon increasing DPPE content, for the DOPC vesicles. In DPPC vesicles, such rafts will not be created as both DPPC and DPPE contain the same aliphatic lipid tails. Therefore, their interaction with cholesterol will be equally strong. It has to be kept in mind, however, that the model membranes only contain 64 lipids in each leaflet, which makes it difficult to mimic the actual raft formation process that could take place in the vesicle systems.

A combination of different processes discussed above (lipid oxidation and raft formation) can also explain the anomaly observed in Figure 4; i.e., why are DPPC vesicles containing 0 mol% DPPE and 25 mol% cholesterol are more vulnerable to ROS ingress compared to the DOPC equivalent? As discussed above, increasing the cholesterol fraction reduces oxidation in DOPC vesicles, whereas it increases oxidation in DPPC vesicles. Moreover, because the DOPC vesicles lack DPPE, raft formation will not occur. This means that the cholesterol molecules are dispersed homogeneously through the membrane, protecting it from pore formation after lipid oxidation of DOPC. On the other hand, in DPPC vesicles, cholesterol itself is oxidised due to impinging ROS, thereby losing its ability to strengthen the membrane.

3.4 CAP jet induced DNA strand breaks

Finally, we investigate the ability of CAP to induce DNA strand breaks of a MB encapsulated within vesicles, focusing on the effect of cholesterol in combination with the saturation degree of the lipids. Therefore, only vesicles 1, 3, 4 and 6 were taken into account, which contain either 10 or 25 mol% cholesterol, 5 mol% DPPE, combined with either DPPC or DOPC. The fluorescence intensity of the MB encapsulated in these vesicles was measured after 60 s of CAP jet treatment. A higher fluorescence intensity correlates with an increased number of DNA strand breaks induced by the CAP jet treatment. The results of these measurements are shown in Figure 9.

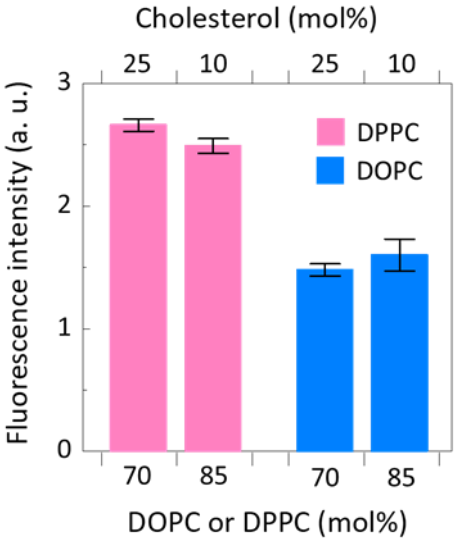

Figure 9: Relative amount of DNA strand breaks within vesicles following 60 s CAP jet treatment of DPPC (pink bars) or DOPC vesicles (blue bars), with a membrane cholesterol content of 10 mol% and 25 mol%, and a fixed DPPE content of 5 mol%.

Upon altering the saturation degree of the main lipid that comprises the vesicle, cholesterol was observed to have opposite effects on the ability of the CAP jet to induce DNA strand breaks within the vesicles. Although the differences are rather small, this observation is in line with that of the ROS measurements discussed above. In the vesicles comprising mainly of a saturated lipid, i.e., containing mostly DPPC, increasing the cholesterol content increases the number of DNA strand breaks, just as it increases the total ROS ingress, due to passive ROS diffusion. On the other hand, in the DOPC vesicles, increasing the cholesterol content leads to a decrease in the number of DNA strand breaks, attributed to the lower DOPC content, and thus less lipid oxidation, yielding less pore formation.

A perhaps somewhat surprising result, is that the total number of DNA strand breaks is significantly lower in the DOPC vesicles compared to the DPPC vesicles, which does not correlate with the total ROS ingress measured in the DCFH vesicle experiments (see Figure 4). Short-lived ROS (e.g. the $^{\bullet}$OH or O-atoms, with an intracellular half-life of 10^{-9} s) are much more effective species to induce DNA strand breaks, rather than long-lived ROS (e.g. H_2O_2, with an intracellular half-life of 10^{-3} s). [29,55] Therefore we need to consider how these short-lived, reactive species are likely to interact with the different components of the vesicle membrane. In DOPC vesicles, the double bonds of the DOPC lipids serve as a highly-reactive site, effectively scavenging these short-lived ROS before they can reach the vesicle interior. [50] The ROS measurements discussed above, measure the total number of ROS (and RNS) entering the vesicles, without differentiating between species with different lifetimes. The combination of both assays (DCFH and MB) indicates that in DOPC vesicles, more ROS are able to penetrate the vesicle membrane, but we surmise these are mostly longer-lived ROS, while in DPPC vesicles, a lower number of ROS is able to diffuse through the membrane, but these are mostly shorter-lived ROS. Generally, the latter are much smaller, which facilitates their ability to diffuse through the membrane. Indeed, previous research has shown that the energy barrier

for passive diffusion across a membrane of short-lived ROS, such as OH or HO_2 radicals, is significantly lower compared to that of e.g., H_2O_2. [51]

4. Conclusion

CAP jet treatment of lipid vesicles was combined with MD simulations to study the effect of different membrane lipid compositions on the ability of plasma-derived ROS to diffuse through these membranes. We varied the saturation degree of the lipid tails, the cholesterol content of the membrane, and the type of lipid head group (i.e., PE vs. PC head group). We selected these characteristics because different cell types, including healthy and cancerous human cells, sometimes also show variations in these types of lipid characteristics, as explained in the Introduction. [9,11–14,56]

Our results indicate that CAP jets can potentially be utilised to induce specific cellular effects (oxidative stress and DNA damage) by targeting interactions of plasma-derived ROS with specific cell membrane lipid components. The ROS measurements show that generally vesicles containing more unsaturated lipids (DOPC) are significantly more vulnerable to ROS ingress compared to those containing more saturated lipids (DPPC). However, adding cholesterol to both types of vesicles makes the DOPC vesicles less vulnerable, while it increases the vulnerability of DPPC vesicles to ROS ingress. Similarly, the addition of DPPE, which contains a smaller head group compared to DOPC and DPPC, also exerts opposite effects in either the DOPC or the DPPC vesicles. In DOPC membranes, the addition of DPPE makes the vesicles more susceptible to ROS permeation, whereas in DPPC membranes, it has a ‘protecting’ role. To determine possible underlying mechanisms causing these observations, we performed MD simulations. Although these simulations cannot be seen as absolute evidence for the underlying mechanisms, they show that multiple effects can potentially play a role, including (i) lipid oxidation of unsaturated phospholipids and cholesterol, (ii) lipid packing due to the head group volume, and (iii) formation of lipid rafts due to strong interactions between lipids of the same type.

We also assessed the ability of a CAP jet to induce DNA strand breaks within vesicles encapsulating a MB. This led to the surprising observations that, although DOPC vesicles are more susceptible to ROS permeation compared to DPPC vesicles, the MB within DPPC vesicles is more susceptible to CAP jet-derived ROS damage. This can be explained by the fact that the double bonds present in DOPC serve as scavenging sites for short-lived ROS, thereby preventing them from entering the vesicle interior. On the other hand, due to the reaction of the double bonds with these short-lived species, the polarity of the bilayer interior increases, facilitating the overall permeation of other impinging ROS. In DPPC vesicles, no reactive sites are present, which allows short-lived ROS to diffuse through the membrane. Once they reach the vesicle interior, these species are very efficient in inducing DNA strand breaks. However, without lipid oxidation occurring, the membrane’s hydrophobic environment is sustained, thereby hindering the overall ingress of impinging larger and more stable ROS (e.g., H_2O_2).

In the past decades, numerous claims have been made for the potential of plasma medicine to help alleviate a wide range of healthcare challenges, which include the selective treatment of cancers[16,57]

However, the full clinical benefits of CAP are yet to be realised, possibly due to our lack in understanding of how CAP can be used to target desired effects in specific cell types. This paper aimed to provide new insights into how different membrane lipid components, of relevance for treatment of certain diseases such as some cancers, can be exploited by CAP technology for targeted membrane therapy. As the oxidative stress provoked by CAP is considered the main mode-of-action to induce cellular effects, it is important to develop our understanding of how the cell membrane landscape influences the cell's response to oxidative stress. To aid this research, more advanced models will need to be developed both experimentally and computationally, as a means of scientifically testing the potential of CAP technologies in biology and medicine.

Acknowledgements

We acknowledge financial support from the Research Foundation – Flanders (FWO), grant numbers 11U5416N, 1200216N and 1200219N, as well as an FWO travel grant to the University of South Australia. The computational work was carried out using the Turing HPC infrastructure at the CalcUA core facility of the Universiteit Antwerpen (UA), a division of the Flemish Supercomputer Centre VSC, funded by the Hercules Foundation, the Flemish Government (department EWI) and the UA. JSO acknowledges the MEXT-Supported Program for the Strategic Research Foundation at Private Universities (S1511021). The authors wish to thank Prof. Hiroshi Akatsuka at Tokyo Institute of Technology for providing a spectrum simulator of the N_2 second positive system. S.-H.H, N.G. and E.J.S acknowledge financial support from the Australian Research Council through Discovery Project Number DP16010498.

References

[1] Escribá P V 2006 Membrane-lipid therapy : a new approach in molecular medicine *Trends Mol. Med.* **12** 34–43

[2] Escribá P V, González-Ros J M, Goñi F M, Vigh L, Sánchez-magraner L, Fernández A M, Busquets X, Horváth I and Barceló-coblijn G 2008 Membranes : a meeting point for lipids , proteins and therapies *Transl. Med.* **12** 829–75

[3] Tan L T, Chan K, Pusparajah P, Lee W, Chuah L, Khan T M, Lee L, Goh B, Pace S and Lee L 2017 Targeting Membrane Lipid a Potential Cancer Cure ? *Front. Pharmacol.* **8** 1–6

[4] Leite B, Aufderhorst-roberts A, Palma M S, Connell S D, Neto R and Beales P A 2015 PE and PS Lipids Synergistically Enhance Membrane Poration by a Peptide with Anticancer Properties *Biophys. J.* **109** 936–47

[5] Martínez J, Oliver V, Casa J, Barcel F, Alemany R, Prades J, Nagy T, Baamonde C, Kasprzyk P G, Terés S, Saus C and Escriba P V 2005 Membrane Structure Modulation , Protein Kinase Cα Activation , and Anticancer Activity of Minerval *Mol. Pharmacol.* **67** 531–40

[6] Sud M, Fahy E, Cotter D, Brown A, Dennis E A, Glass C K, Jr A H M, Murphy R C and Raetz C R H 2007 LMSD : LIPID MAPS structure database *Nucleic Acids Res.* **35** 527–32

[7] van Meer G 1989 Lipid traffic in animal cells *Annu. Rev. Cell Biol.* **5** 247–78

[8] Alberts B, Johnson A, Lewis J, Raff M, Roberts K and Walter P 2008 *Molecular biology of the cell* (Garland Science)

[9] Shinitzky M 1984 Membrane fluidity in malignancy *Biochim. Biophys. Acta* **738** 251–61

[10] Taraboletti G, Perin L, Bottazzi B, Mantovani A, Giavazzi R and Salmona M 1989 Membrane fluidity affects tumor - cell motility, invasion and lung-colonizing potential *Int. J. Cancer* **44** 707–7013

[11] Bernardes N and Fialho A M 2018 Perturbing the Dynamics and Organization of Cell Membrane Components : A New Paradigm for Cancer-Targeted Therapies *Int. J. Mol. Sciiences* **19** 3871

[12] Papadopoulos M C and Saadoun S 2015 Key roles of aquaporins in tumor biology *Biochim. Biophys. Acta - Biomembr.* **1848** 2576–83

[13] Saadoun S, Papadopoulos M C, Davies D C, Bell B A and Krishna S 2002 Increased aquaporin I water channel expression in human brain tumours *Br. J. Cancer* **87** 621–3

[14] van Blitterswijk W J, de Veer G, Krol J H and Emmelot P 1982 Comparative lipid analysis of purified plasma membranes and shed extracellular membrane vesicles from normal murine thymocytes and leukemic GRSL cells *BBA - Biomembr.* **688** 495–504

[15] Ozben T 2007 Oxidative Stress and Apoptosis: Impact on Cancer Therapy *J. Pharm. Sci.* **96** 2181–96

[16] Keidar M, Walk R, Shashurin A, Srinivasan P, Sandler A, Dasgupta S, Ravi R, Guerrero-Preston R and Trink B 2011 Cold plasma selectivity and the possibility of a paradigm shift in cancer therapy. *Br. J. Cancer* **105** 1295–301

[17] Ratovitski E A, Cheng X, Yan D, Sherman J H, Canady J, Trink B and Keidar M 2014 Anti-cancer therapies of 21st century: Novel approach to treat human cancers using cold atmospheric plasma *Plasma Process. Polym.* **11** 1128–37

[18] Kakei R, Ogino A, Iwata F and Nagatsu M 2010 Production of ultrafine atmospheric pressure plasma jet with nano-capillary *Thin Solid Films* **518** 3457–60

[19] Kim J Y, Wei Y, Li J, Foy P, Hawkins T, Ballato J and Kim S 2011 Single-Cell-Level Microplasma Cancer Therapy *Small* **7** 2291–5

[20] Laroussi M 2018 Plasma Medicine : A Brief Introduction *Plasma* **1** 47–60

[21] Keidar M 2015 Plasma for cancer treatment *Plasma Sources Sci. Technol.* **24** 033001

[22] Graves D B 2012 The emerging role of reactive oxygen and nitrogen species in redox biology and some implications for plasma applications to medicine and biology *J. Phys. D. Appl. Phys.* **45** 263001

[23] Chan Y-H M and Boxer S G 2007 Model Membrane Systems and Their Applications *Curr. Opin. Chem. Biol.* **11** 581–7

[24] Svarnas P, Matrali S H, Gazeli K and Antimisiaris S G 2015 Assessment of Atmospheric-Pressure Guided Streamer (Plasma Bullet) Influence on Liposomes with Different Composition and Physicochemical Properties *Plasma Process. Polym.* **12** 655–65

[25] Van Der Paal J, Neyts E C, Verlackt C C W and Bogaerts A 2015 Effect of lipid peroxidation on membrane permeability of cancer and normal cells subjected to oxidative

stress *Chem. Sci.* **7** 489–98

[26] Metelmann H R, Seebauer C, Miller V, Fridman A, Bauer G, Graves D B, Pouvesle J M, Rutkowski R, Schuster M, Bekeschus S, Wende K, Masur K, Hasse S, Gerling T, Hori M, Tanaka H, Ha Choi E, Weltmann K D, Metelmann P H, Von Hoff D D and Woedtke T von 2018 Clinical experience with cold plasma in the treatment of locally advanced head and neck cancer *Clin. Plasma Med.* **9** 6–13

[27] Veal E A, Day A M and Morgan B A 2007 Hydrogen Peroxide Sensing and Signaling *Mol. Cell* **26** 1–14

[28] Bekeschus S, Kolata J, Winterbourn C, Kramer A, Turner R, Weltmann K D, Br B and Masur K 2014 Hydrogen peroxide : A central player in physical plasma-induced oxidative stress in human blood cells *Free Radic Res.* **48** 542–9

[29] Szili E J, Gaur N, Hong S-H, Kurita H, Oh J-S, Ito M, Mizuno A, Hatta A, Cowin A J, Graves D and Short R D 2017 The assessment of cold atmospheric plasma interactions with DNA in synthetic models of tissue fluid, tissue and cells *J Phys D Appl Phys* **50** 274001

[30] Meer G Van, Voelker D R and Feigenson G W 2008 Membrane lipids : where they are and how they behave *Nat. Rev.* **9** 112–24

[31] Harayama T and Riezman H 2018 Understanding the diversity of membrane lipid composition *Nat. Publ. Gr.* **19** 281–96

[32] Rivel T, Ramseyer C and Yesylevskyy S 2019 The asymmetry of plasma membranes and their cholesterol content influence the uptake of cisplatin *Sci. Rep.* **9** 5627

[33] Kurita H, Nakajima T, Yasuda H and Takashima K 2011 Single-molecule measurement of strand breaks on large DNA induced by atmospheric pressure plasma jet *Appl. Phys. Lett.* **99** 191504

[34] Razzokov J, Yusupov M, Cordeiro R M and Bogaerts A 2018 Atomic scale understanding of the permeation of plasma species across native and oxidized membranes *J. Phys. D. Appl. Phys.* **51** 365203

[35] Yusupov M, Van der Paal J, Neyts E C and Bogaerts A 2017 Synergistic effect of electric field and lipid oxidation on the permeability of cell membranes *BBA - Gen. Subj.* **1861** 839–47

[36] Oh J, Aranda-gonzalvo Y and Bradley J W 2011 Time-resolved mass spectroscopic studies of an atmospheric-pressure helium microplasma jet *J Phys D Appl Phys* **44** 365202

[37] Gaydon A G 1976 *The Identification of Molecular Spectra* (Springer Netherlands)

[38] Koike S, Sakamoto T, Kobori S, Matsuura H and Akatsuka H 2004 Spectroscopic Study on Vibrational Nonequilibrium of a Microwave Discharge Nitrogen Plasma *Jpn. J. Appl. Phys.* **43** 5550–7

[39] Kurihara J, Iwagami N and Oyama K 2013 N2 Temperature of vibration instrument for sounding rocket observation in the lower thermosphere *TERRAPUB* 33–9

[40] Oh J, Furuta H, Hatta A and Bradley J W 2015 Investigating the effect of additional gases in an atmospheric-pressure helium plasma jet using ambient mass spectrometry *Jpn. J. Appl. Phys.* 01AA03

[41] Oh J, Kakuta M, Furuta H, Akatsuka H and Hatta A 2016 Effect of plasma jet diameter on the efficiency of reactive oxygen and nitrogen species generation in water *Jpn. J.*

Appl. Phys. 06HD01

[42] Oh J, Szili E J, Gaur N and Hong S 2016 How to assess the plasma delivery of RONS into tissue fluid and tissue *J. Phys. D. Appl. Phys.* **49** 304005

[43] Kim H Y, Hong Y J, Baik K Y, Kwon G C, Choi J J, Cho G S, Han Sup U, Kim D Y and Choi E H 2014 Measurement of Reactive Hydroxyl Radical Species Inside the Biosolutions During Non-thermal Atmospheric Pressure Plasma Jet Bombardment onto the Solution *Plasma Chem Plasma Process* 457–72

[44] Attri P, Kim Y H, Park D H, Park J H, Hong Y J, Uhm H S, Kim K, Fridman A and Choi E H 2015 Generation mechanism of hydroxyl radical species and its lifetime prediction during the plasma-initiated ultraviolet (UV) photolysis *Sci. Rep.* 9332

[45] Traylor M J, Pavlovich M J, Karim S, Hait P, Sakiyama Y, Clark D S and Graves D B 2011 Long-term antibacterial efficacy of air plasma-activated water *J. Phys. D. Appl. Phys.* 472001

[46] Ercan U K, Wang H, Ji H, Fridman G, Brooks A D and Joshi S G 2013 Nonequilibrium Plasma-Activated Antimicrobial Solutions are Broad-Spectrum and Retain their Efficacies for Extended Period of Time y *Plasma Process. Polym.* 544–55

[47] Halliwell B and Gutteridge J M C 2015 *Free Radicals in Biology and Medicine.pdf* (Oxford University Press)

[48] Pelicano H, Carney D and Huang P 2004 ROS stress in cancer cells and therapeutic implications *Drug Resist. Updat.* **7** 97–110

[49] Silvius J R 1982 *Thermotropic Phase Transitions of Pure Lipids in Model Membranes and Their Modifications by Membrane Proteins* (New York: John Wiley & Sons, Inc.)

[50] Lloyd A C, Darnall K R, Winer A M and Pitts J N J 1976 Relative Rate Constants of the Hydroxyl Radical with a Series of Alkanes, Alkenes, and Aromatic Hydrocarbons Alan *J. Phys. Chem.* **80** 789–94

[51] Van der Paal J, Verheyen C, Neyts E C and Bogaerts A 2017 Hampering Effect of Cholesterol on the Permeation of Reactive Oxygen Species through Phospholipids Bilayer : Possible Explanation for Plasma Cancer Selectivity *Sci. Rep.* **7** 39526

[52] Yusupov M, Wende K, Kupsch S, Neyts E C, Reuter S and Bogaerts A 2017 Effect of head group and lipid tail oxidation in the cell membrane revealed through integrated simulations and experiments *Sci. Rep.* **7** 5761

[53] Neto A J P and Cordeiro R M 2016 Molecular simulations of the effects of phospholipid and cholesterol peroxidation on lipid membrane properties *BBA - Biomembr.* **1858** 2191–8

[54] Sezgin E, Lavental I, Mayor S and Eggeling C 2017 The mystery of membrane organization: composition, regulation and physiological relevance of lipid rafts *Nat Rev Mol Cell Biol.* **18** 361–74

[55] Dickinson B C and Chang C J 2012 Chemistry and biology of reactive oxygen species in signaling or stress responses *Nat Chem Biol.* **7** 504–11

[56] Liu Q, Luo Q, Halim A and Song G 2017 Targeting lipid metabolism of cancer cells : A promising therapeutic strategy for cancer *Cancer Lett.* **401** 39–45

[57] Kim S J and Chung T H 2016 Cold atmospheric plasma jet- generated RONS and their selective effects on normal and carcinoma cells *Sci. Rep.* **6** 20332

[58] Abraham M J, Murtola T, Schulz R, Pall S, Smith J C, Hess B and Lindah E 2015 Gromacs: High performance molecular simulations through multi-level parallelism from laptops to supercomputers *SoftwareX* **1-2** 19–25

[59] Schmid N, Eichenberger A P, Choutko A, Riniker S, Winger M, Mark A E and Van Gunsteren W F 2011 Definition and testing of the GROMOS force-field versions 54A7 and 54B7 *Eur. Biophys. J.* **40** 843–56

[60] Berendsen H J, Postma P J, van Gunsteren W F and Hermans J 1981 *Interaction Models for Water in Relation to Protein Hydration* ed B Pulmann (Dordrecht: Springer)

[61] Poger D and Mark A E 2010 On the Validation of Molecular Dynamics Simulations of Saturated and cis -Monounsaturated Phosphatidylcholine Lipid Bilayers : A Comparison with Experiment *J. Chem. Theory Comput.* **6** 325–36

[62] Poger D, Gunsteren W F V A N and Mark A E 2009 A New Force Field for Simulating Phosphatidylcholine Bilayers *J. Comput. Chem.* **31** 1117–25

[63] Piggot T J, Holdbrook D A and Khalid S 2011 Electroporation of the E . coli and S . Aureus Membranes : Molecular Dynamics Simulations of Complex Bacterial Membranes *J. Phys. Chem. B* **115** 13381–8

[64] Cordeiro R M 2014 Reactive oxygen species at phospholipid bilayers: Distribution, mobility and permeation *Biochim. Biophys. Acta - Biomembr.* **1838** 438–44

[65] Martínez L, Andrade R, Birgin E G and Martínez J M 2009 Packmol: A Package for Building Initial Configuration forMolecular Dynamics Simulations *J. Comput. Chem.* **30** 2157–64

[66] Piggot T J, Pineiro A and Khalid S 2012 Molecular Dynamics Simulations of Phosphatidylcholine Membranes : A Comparative Force Field Study *J. Chem. Theory Comput.* **8** 4593–609

[67] Parrinello M and Rahman A 1981 Polymorphic transitions in single crystals: A new molecular dynamics method *J. Appl. Phys.* **52** 7182–90

[68] Hoover W G 1985 Canonical dynamics: Equilibrium phase-space distributions *Phys. Rev. A* **31** 1695–7

[69] Essmann U, Perera L, Berkowitz M L, Darden T, Lee H and Pedersen L G 1995 A smooth particle mesh Ewald method *J Chem Phys* **103** 8577–93

[70] Piggot T J, Piñeiro Á and Khalid S 2012 Molecular Dynamics Simulations of Phosphatidylcholine Membranes : A Comparative Force Field Study School of Chemistry , *J. Chem. Theory Comput.* **8** 4593–609

[71] Nagle J F 1993 Area/lipid of bilayers from NMR *Biophys. J.* **64** 1476–81

[72] Kučerka N, Nagle J F, Sachs J N, Feller S E, Pencer J, Jackson A and Katsaras J 2008 Lipid bilayer structure determined by the simultaneous analysis of neutron and X-ray scattering data *Biophys. J.* **95** 2356–67

[73] Pan J, Tristram-Nagle S, Kučerka N and Nagle J F 2008 Temperature dependence of structure, bending rigidity, and bilayer interactions of dioleoylphosphatidylcholine bilayers *Biophys. J.* **94** 117–24

[74] Torrie G M and Valleau J P 1977 Nonphysicl Sampling Distributions in Monte Carlo Free-Energy Estimation: Umbrella Sampling *J. Comput. Phys.* **23** 187–99

[75] Kästner J 2011 Umbrella sampling *WIREs Comput. Mol. Sci.* **1** 932–42

[76] Hub J S, Groot B L De and Spoel D Van Der 2010 g _ wham - A Free Weighted Histogram Analysis Implementation Including Robust Error and Autocorrelation Estimates *J. Chem. Theory Comput.* **6** 3713–20

Appendix A: Experimental details

A1. Preparation of buffers

The 4-(2-hydroxyethyl)-1-piperazineethanesulfonic acid (HEPES) buffer was prepared by dissolving the following components in 100 mL of purified water:

- HEPES—238.3 mg
- NaCl—624 mg
- NaOH—22.4 mg
- EDTA—29.22 mg

The pH of the solution was adjusted to 7.4 with 10 mM NaOH solution. The buffer was filtered through a 0.2 µm syringe filter before use. HEPES buffer was used for the preparation and dilution of the vesicles for the experiments.

A concentrated buffer of 1M Tris buffer was prepared by dissolving 12.11 g of Tris-base in 80 mL water. The pH was adjusted to 7.6 by adding concentrated HCl (6.2 M), after which the final volume was adjusted to 100 mL. The concentrated Tris buffer was diluted to 10 mM in water for the preparation of the molecular beacon (MB) stock solution.

A2. ortho-phenylenediamine (OPD)/horseradish peroxidase (HRP) H_2O_2 indicator

Ortho-phenylenediamine OPD (Sigma-Aldrich, P9187) was dissolved in 20 mL of PBS supplemented with 125 ng /ml of horseradish peroxidase (HRP) (Sigma-Aldrich, catalogue number P6782). The solution was stored at 4 °C until use. The OPD/HRP solution was used to determine the concentration of H_2O_2 generated by the CAP jet in solution. This involved adding 200 µL of the OPD/HRP solution to wells of a 96-well plate and then treating the solution with the CAP jet. After 10 min of incubation at ambient temperature (to allow time for the HRP to catalyse the oxidation of the OPD in the presence of H_2O_2, into a yellow coloured product), 100 µL of the OPD/HRP solution was transferred to a fresh 96-well plate for measurement. The H_2O_2 concentration in the plasma jet treated was determined according to a calibration curve (see below).

A3. Determination of H_2O_2 concentration

The H_2O_2 concentration generated by the CAP jet treatments in the HEPES buffer (presented in Figure 3d in the manuscript) was determined according to a calibration curve. The calibration curve was determined by adding 10 µL of known H_2O_2 concentrations to 80 µL of OPD/HRP solution (see above) and incubating for 10 min at ambient temperature (same incubation time as is used in the manuscript, which was determined to be sufficient to develop the solution). Afterwards, absorbance of the OPD solution was recorded on a microplate reader, as described in section 2.5 of the manuscript. The absorbance data were plotted as function of the H_2O_2 concentration as shown in Figure A1.1 below. The data covered the full range of absorbance data (both below and above) achieved by the CAP jet treatments. The calibration curve was near linear ($R^2 = 0.9987$) with the equation from the curve ($y = 0.1043x$) used to derive the unknown H_2O_2 concentration produced by the CAP jet treatments.

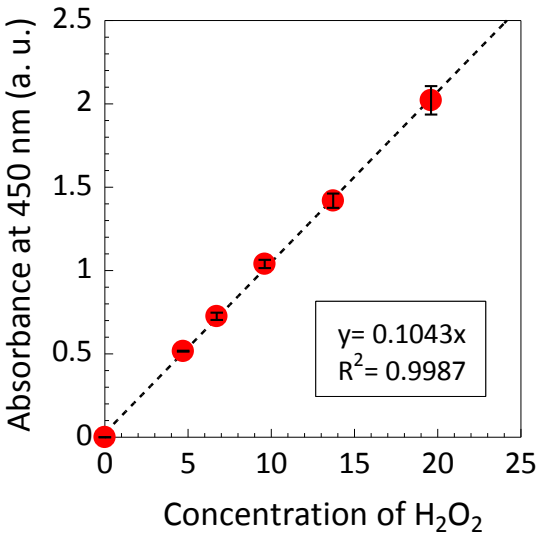

Figure A1.1. Calibration curve used to derive the H_2O_2 concentration produced in the CAP jet treated HEPES solution, as shown in Figure 3d in the manuscript.

A4. Carboxyfluorescein (CF): assessment of vesicle rupture

Vesicles encapsulating CF were used to analyse the possibility of the vesicle membrane being ruptured by the CAP jet treatment. In these experiments, 50 mM of CF was encapsulated within the vesicles, at which concentration CF is self-quenched inside the intact vesicles. However, if the vesicles were ruptured by the CAP jet treatment, the CF would be released and diluted into the HEPES buffer containing the vesicles, resulting in a switch-on of fluorescence (i.e. a positive indication of vesicle rupture). To prepare a 50 mM concentration of the carboxyfluorescein (CF) encapsulation buffer, the following components were dissolved in 13 mL of purified water:

- CF — 244 mg
- NaCl — 7.6 mg
- NaOH — 70.2 mg
- HEPES — 31 mg
- EDTA — 3.7 mg

The pH was adjusted to 7.4, and the solution was stored shielded from ambient light at 4 °C until use. Figure A1.2 shows the results of a typical vesicle rupture assay for vesicles encapsulating CF. This figure shows the results of a 2 min CAP jet treatment of a vesicle system 10 (50 mol% DOPC, 25 mol% DPPE and 25 mol% cholesterol - see Table 1 in manuscript), which is harsher than any treatment conditions used in the paper. As seen in Figure A1.2, there was no increase in the CF fluorescence signal even after this more pro-longed plasma CAP jet treatment. As a positive control, Triton X-100 was added to completely lyse the vesicles, which was seen by a prominent increase in fluorescence (Figure A1.2).

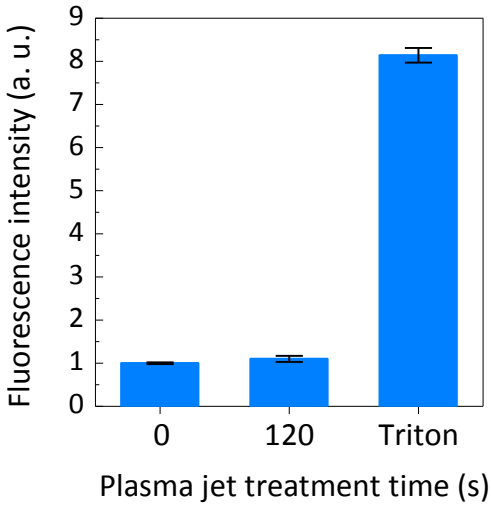

Figure A1.2**.** Result of a typical assay to assess vesicle rupture by CAP plasma jet treatment. The vesicle membrane composition comprised of 50 mol% DOPC, 25 mol% DPPE and 25 mol% cholesterol (vesicle system 10, Table 1 in manuscript). Positive control of vesicle rupture was Triton X-100.

Appendix B: Computational details

B1. System set-up and equilibration

All simulations, i.e., energy minimization, equilibration and umbrella sampling runs, were performed using the GROMACS-5.1 package [58]. For the interatomic interactions the GROMOS 54A7 force field parameters were applied [59] in combination with the SPC water model [60]. Specifically, the GROMOS-type parameters for the DOPC, DPPC, DPPE, cholesterol and H_2O_2 molecules were adopted from [61], [62], [63], [53] and [64], respectively. After constructing the initial configurations using the Packmol package [65], an energy minimization of all systems was performed using the steepest-descent algorithm. After the energy minimization, all systems were equilibrated for 400 ns in the NPT ensemble (i.e., constant number of particles, pressure and temperature). The temperature at which the systems were equilibrated was different for systems containing either DOPC or DPPC, i.e., at 298 K or 323 K, respectively. These temperatures were chosen based on the transition temperatures of both lipids (253 K for DOPC and 314 K for DPPC), to ensure that all simulated bilayers were in the liquid state, as was the case with the vesicles studied experimentally. [66] The reference pressure used in the simulations was the same for all bilayers, i.e., 1 atmosphere. The NPT ensemble was employed using the Parrinello-Rahman barostat [67] with compressibility and coupling constant of 4.5×10^{-5} bar^{-1} and 2 ps, respectively, as well as the Nose–Hoover thermostat [68] with a coupling constant of 0.5 ps. Considering the non-bonded interactions, the particle mesh Ewald method was used to treat electrostatic interactions with cut-off radius of 1.0 nm for Coulomb interactions. [69] The same cut-off radius was applied for the van der Waals interactions. This cut-off radius was chosen after scanning different values and evaluating the results based on the agreement of the obtained area per lipid with experimental values (0.63 nm^2 for both DOPC and DPPC bilayers in native form, see [70–73] and references therein). All simulations were carried out using a time step of 2 fs, and periodic boundary conditions were applied in all three directions.

B2. Umbrella sampling (US) simulations

To investigate the ability of H_2O_2 permeation through the different bilayers, US simulations were performed to determine free energy profiles (FEPs) of H_2O_2 across all systems. [74,75] From the last 40 ns of the equilibration run, five membrane structures were extracted, which served as the initial configurations for the US runs. In each US simulation, 32 H_2O_2 molecules were added to the structure, distributed over eight layers along the bilayer normal (i.e. four molecules in each plane). These molecules were restrained to move along the *z*-axis by a harmonic bias with force constant of 2000 $kJ.mol^{-1}.nm^{-2}$. Furthermore, their movement in the *xy*-plane was also restrained by using the so-called flat-bottomed position restraint, with a radius of 0.5 nm and a force constant of 500 $kJ.mol^{-1}.nm^{-2}$. To obtain a FEP, 160 US windows were used, which were separated by 0.5 Å. The US simulations were performed in the NPT ensemble, with the same parameters as in the equilibration runs. The total simulation time of these runs was 5 ns, of which the last 2 ns were used as sampling time. The convergence of the free energy results was evaluated based on the symmetricity of the profiles to the centre of the bilayer. From each initial structure, four different FEPs were obtained (one for each H_2O_2 molecule placed in each US window). By using five different initial structures (see above), a total of

20 FEPs was obtained for each bilayer composition. These profiles were averaged, leading to the FEPs shown in the Figure 5 of the manuscript. Each FEP was calculated using a periodic version of the weighted histogram analysis method (WHAM), by utilizing the *gmx wham* tool of GROMACS. [76]